

Emergent XY electronic nematicity in iron-based superconductors

K. Ishida,^{1,*} M. Tsujii,^{1,*} S. Hosoi,^{1,†} Y. Mizukami,¹ S. Ishida,² A. Iyo,² H. Eisaki,²
T. Wolf,³ K. Grube,³ H. v. Löhneysen,³ R. M. Fernandes,⁴ and T. Shibauchi¹

¹*Department of Advanced Materials Science, University of Tokyo, Kashiwa, Chiba 277-8561, Japan*

²*Electronics and Photonics Research Institute, National Institute of Advanced*

Industrial Science and Technology, Tsukuba, Ibaraki 305-8568, Japan

³*Institut für Festkörperforschung, Karlsruher Institut für Technologie, 76021 Karlsruhe, Germany*

⁴*School of Physics and Astronomy, University of Minnesota, Minneapolis, Minnesota 55455, U.S.A.*

Electronic nematicity, a correlated state that spontaneously breaks rotational symmetry, is observed in several layered quantum materials. In contrast to their liquid-crystal counterparts, the nematic director cannot usually point in an arbitrary direction (XY nematics), but is locked by the crystal to discrete directions (Ising nematics), resulting in strongly anisotropic fluctuations above the transition. Here, we report on the observation of nearly isotropic XY-nematic fluctuations, via elastoresistance measurements, in hole-doped $\text{Ba}_{1-x}\text{Rb}_x\text{Fe}_2\text{As}_2$ iron-based superconductors. While for $x = 0$ the nematic director points along the in-plane diagonals of the tetragonal lattice, for $x = 1$ it points along the horizontal and vertical axes. Remarkably, for intermediate doping, the susceptibilities of these two symmetry-irreducible nematic channels display comparable Curie-Weiss behavior, thus revealing a nearly XY-nematic state. This opens a new route to assess this elusive electronic quantum liquid-crystalline state, which is a candidate to host unique phenomena not present in the Ising-nematic case.

I. INTRODUCTION

Liquid crystals are composed of molecules with anisotropic shapes, which possess a degree of orientational order. As a result, they can form nematic phases, in which translational invariance is preserved, but rotational symmetry is spontaneously broken by the selection of a director along which the molecules align. Strongly correlated electron systems often show exotic states of matter analogous to liquid-crystalline states, originating from nontrivial quantum many-body interactions. In particular, electronic nematic phases have been found in a number of quantum materials and have generated a lot of attention [1, 2]. After its original experimental identification in quantum Hall systems [3], electronic nematicity has increasingly been recognized as a ubiquitous feature of unconventional superconductors. In iron-based superconductors, electronic nematic order and fluctuations span a wide region of the phase diagram [4, 5], and likely impact superconductivity [6]. Electronically-driven rotational symmetry breaking has also been reported inside the mysterious pseudogap phase of high- T_c cuprates [7–9] as well as in the elusive hidden-order phase of the heavy-fermion material URu_2Si_2 [10].

A crucial difference between electronic and liquid-crystalline nematic orders is that the former develops in the presence of a crystal, which by itself does break the rotational symmetry of the system – for instance, by restricting the possible paths along which the electrons can hop. As a result, while in liquid crystals the nematic director can point anywhere in space (i.e., it has a

continuous symmetry), in electronic systems it is generally restricted to a few high-symmetry directions of the crystal (i.e., it has a discrete symmetry). While such a discrete electronic nematic state still displays interesting properties [1, 2], a hypothetical continuous electronic nematic state would host several unique quantum many-body phenomena [11]. For instance, the transverse and longitudinal fluctuations in the disordered phase have completely different dynamics, which may lead to multi-scale critical behavior [12]. Moreover, the ordered phase has a Goldstone mode associated with the breaking of the continuous symmetry by the director. Remarkably, unlike other Goldstone modes such as phonons or magnons, the nematic mode couples directly to the electronic density rather than to gradients of the density [13]. This can lead to strange metallic behavior [11] and strongly impact superconductivity [14].

At first sight, the inevitable presence of the crystal may be taken as an insurmountable obstacle to realize a continuous electronic nematic state in actual materials. However, as we argue now, and demonstrate below experimentally in the hole-doped iron pnictide $\text{Ba}_{1-x}\text{Rb}_x\text{Fe}_2\text{As}_2$, a nearly-continuous nematic phase can be observed under certain conditions. To make the discussion concrete, we consider layered crystals with tetragonal symmetry, i.e., the symmetry of a square. Indeed, many of the materials where nematicity has been observed do possess this symmetry. We start our discussion by first assuming that there was no underlying crystal. Then the electronic nematic director could point anywhere in the layer plane. In this case, in analogy to a two-dimensional nematic liquid crystal, the nematic order parameter is described in terms of a traceless symmetric 2×2 matrix [11] given by: $\mathcal{Q} = \begin{pmatrix} N_1 & N_2 \\ N_2 & -N_1 \end{pmatrix}$. Here, the order parameter N_1 corresponds to a quadrupo-

* These authors contributed equally to this work.

† Present address: Department of Materials Engineering Science, Osaka University, Toyonaka, Osaka 560-8531, Japan.

lar charge density that makes the horizontal (x) and vertical (y) directions inequivalent ($d_{x^2-y^2}$ -wave form factor), whereas N_2 corresponds to a quadrupolar charge density that makes the two diagonal directions inequivalent (d_{xy} -wave form factor). A linear combination of N_1 and N_2 can be constructed such that the quadrupolar charge density can be rotated along any in-plane direction. The static and uniform free energy depends only on traces of even powers of \mathbf{Q} , i.e., only on the combination ($N_1^2 + N_2^2$), reflecting the continuous symmetry of the nematic director. Therefore, N_1 and N_2 can be interpreted as two orthogonal components of the continuous nematic order parameter. Borrowing the nomenclature of magnetic phases, the resulting nematic phase is called an XY-nematic state.

The existence in reality of the tetragonal crystal, of course, dramatically changes this scenario. Now, N_1 and N_2 transform as two different irreducible representations of the tetragonal point group, denoted respectively by B_{1g} and B_{2g} . Phenomenologically, this leads to a term in the free energy that explicitly lifts the degeneracy between N_1 and N_2 , changing the symmetry of the nematic state from XY (continuous) to Ising (discrete). More formally, the free energy expansion becomes

$$F = \frac{\gamma}{2}(N_1^2 - N_2^2) + \frac{a}{2}(N_1^2 + N_2^2) + \frac{u}{4}(N_1^2 + N_2^2)^2. \quad (1)$$

Here, a and u are Landau coefficients that depend on the microscopic model. The anisotropic term γ selects one of the two components of the XY nematic order parameter: B_{1g} nematic order when $\gamma < 0$, and B_{2g} nematic order when $\gamma > 0$. The situation is analogous to an XY (i.e., planar) ferromagnet with an easy-axis anisotropy. Indeed, the nematic order parameter can now be written in terms of Pauli matrices as $\mathbf{Q} = N_1\sigma_z + N_2\sigma_x$, expressing the analogy between N_i and magnetic moment components. In the magnetic analogue, the γ term corresponds to the single-ion anisotropy that defines the magnetization easy axis. This analogy offers a fruitful insight: in ferromagnets, when the single-ion anisotropy is much smaller than the exchange coupling, although the magnetic transition is formally Ising-like, the fluctuation spectrum is very similar to that of the XY ferromagnet, except at very low energies. Moreover, once long-range order sets in, the collective modes correspond essentially to a Goldstone mode with a very small gap.

Thus, going back to the nematic case, it is expected that many of the properties of the XY-nematic state will be relevant to describe the system's behavior over a wide energy range as long as the anisotropy coefficient $|\gamma|$ is much smaller than the nematic energy scale, which we can set to be the nematic transition temperature T_{nem} . The remaining task is to find a concrete system with $|\gamma| \ll T_{\text{nem}}$. A promising strategy is to interpolate between two different compounds that display B_{1g} nematic order ($\gamma < 0$) and B_{2g} nematic order ($\gamma > 0$), forcing γ to cross zero. In the remainder of this paper, we show

that such a situation is realized in the hole-doped iron pnictide $\text{Ba}_{1-x}\text{Rb}_x\text{Fe}_2\text{As}_2$.

II. METHODS

The parent compound BaFe_2As_2 ($x = 0$) displays an antiferromagnetic transition that is preceded by a tetragonal to orthorhombic structural transition, which makes the diagonals [110] and [1̄10] of the tetragonal crystallographic unit cell inequivalent. It is well established that the structural transition is not driven by lattice degrees of freedom [15], but is the result of an electronic nematic instability in the B_{2g} channel along the Fe-Fe direction [Fig. 1(a)]. Note that our notation refers to the crystallographic 2-Fe unit cell; in the 1-Fe unit cell notation sometimes used in the literature, B_{1g} and B_{2g} are exchanged. Upon increasing doping, the structural transition temperature is suppressed, approaching a putative quantum critical point near optimal doping, where the superconducting dome is peaked. The superconducting dome extends all the way up to $x = 1$. Interestingly, in all hole-doped systems $\text{Ba}_{1-x}\text{A}_x\text{Fe}_2\text{As}_2$, with alkali metal $A = \text{K}, \text{Rb}, \text{Cs}$, the effective electronic mass is observed to be strongly enhanced near $x = 1$ [16–19]. This suggests a progressively more important role of electronic correlations in the $3d^{5.5}$ electronic configuration ($x = 1$) as compared to the $3d^6$ configuration ($x = 0$), which may be related to proximity to a hypothetical $3d^5$ Mott insulating state [20, 21]. This motivates a careful investigation of nematic tendencies in extremely hole-doped pnictides by using high-quality single crystals (see Appendix A), with the prospect of finding a suitable alloy series with a crossover to B_{1g} dominance, as the stronger correlations may promote a mechanism for electronic nematicity different from that of the undoped compound [22].

To study nematicity in the extremely hole-doped regime, we use elastoresistance measurements, which have been shown to probe the bare static nematic susceptibility [15, 23, 24]. In this technique, we measure the relative change in resistance $\Delta R/R$ in response to an externally applied strain ϵ , which is controlled by a piezoelectric device. Because uniaxial strain couples linearly to the nematic order parameters, in the linear response regime the quantity $\chi_{\text{nem}} \sim \frac{1}{R} \frac{\partial \Delta R}{\partial \epsilon}$ is proportional to the nematic susceptibility (see Appendix B). Specifically, in the iron pnictides, the nematic susceptibilities in the B_{1g} and B_{2g} symmetry channels (denoted here by $\chi_{\text{nem}}^{[100]}$ and $\chi_{\text{nem}}^{[110]}$, respectively, with the superscript denoting the strain direction) can be obtained by applying strain along the nearest neighbor Fe-As and Fe-Fe bond directions, corresponding to [100] and [110], respectively [Fig. 1(a)].

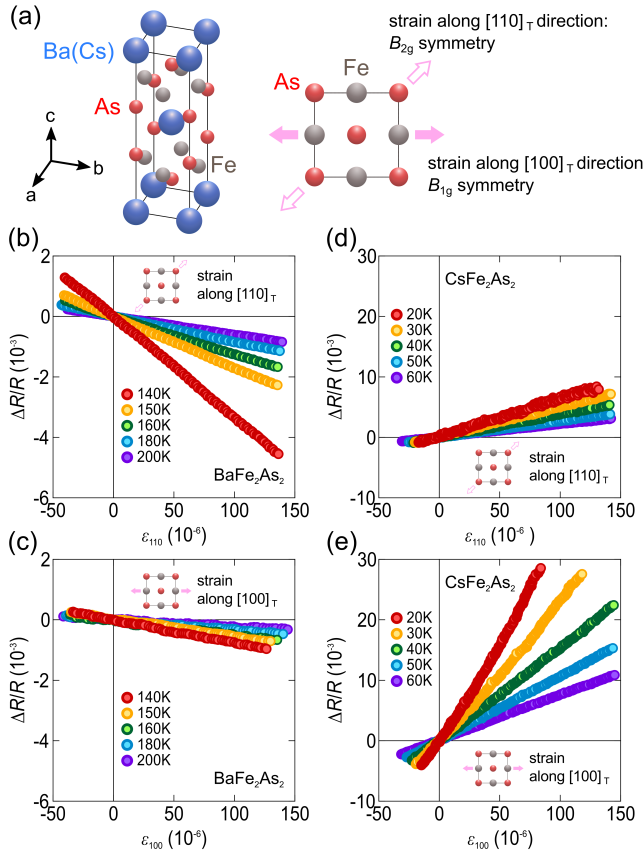


FIG. 1. Elastoresistance under strain for two symmetry channels in AFe₂As₂ ($A = \text{Ba}$ and Cs). (a) Crystal structure of the tetragonal AFe₂As₂ ($A = \text{Ba}$, Cs , or $\text{Ba}_{1-x}\text{Rb}_x$). By applying the strain parallel to the tetragonal [110] or [100] direction (nearest Fe-Fe bond or Fe-As bond direction, respectively), the nematic susceptibilities in the B_{2g} or B_{1g} channels can be extracted. (b),(c) Representative elastoresistance data $\Delta R/R$ of BaFe₂As₂ samples at several temperatures above T_{nem} as a function of strain along [110] (b) and [100] (c) directions. The samples are glued on piezo stacks and the strain is induced by applying voltage to the piezo stacks. The current direction is parallel to the strain direction in both configurations. (d),(e) Similar data for CsFe₂As₂ for the [110] (d) and [100] (e) orientations.

III. RESULTS AND DISCUSSION

Figure 1(b)-(e) shows representative data of $\Delta R/R$ as a function of applied strain ϵ along the [100] and [110] directions. In BaFe₂As₂, which displays the $3d^6$ electronic configuration, the elastoresistances in the two channels show a striking anisotropy, with the response to the strain along the [110] direction being much larger than that along [100] [Fig. 1(b),(c)]. This is consistent with previous reports [15], and reflects the Ising-like character of the B_{2g} nematic state, which sets in when $\chi_{\text{nem}}^{[110]}$ peaks. In sharp contrast, in CsFe₂As₂ with $3d^{5.5}$ electronic configuration, the elastoresistance for strain applied along [100] becomes much larger than that along

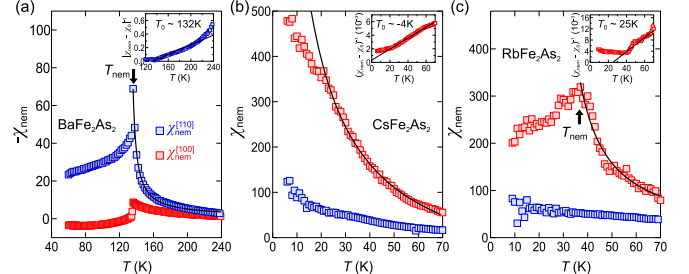


FIG. 2. Temperature dependence of the nematic susceptibility $\chi_{\text{nem}}^{[100]}$ (B_{1g} or Fe-As direction, red squares) and $\chi_{\text{nem}}^{[110]}$ (B_{2g} or Fe-Fe direction, blue squares) in BaFe₂As₂ (a), CsFe₂As₂ (b), and RbFe₂As₂ (c), as determined by the elastoresistance measurements along the [100] and [110] directions. The solid lines are the Curie-Weiss fits for the dominant nematic fluctuations. The insets show the temperature dependence of the inverse susceptibility, whose intercept provides an estimate of the Curie-Weiss temperature T_0 .

[110], indicating that Ising-like B_{1g} nematic fluctuations are dominant. Such a difference can be clearly seen in the temperature dependence of the nematic susceptibilities obtained from the slopes of $\Delta R/R$ as function of ϵ , as shown in Fig. 2(a),(b). Although the nematic susceptibilities presented here were evaluated from longitudinal elastoresistance measurements, we confirmed that they are identical to those determined by using a modified Montgomery method, indicating negligible contaminations of A_{1g} -symmetry strain (see Appendix:B).

In the case of BaFe₂As₂ [Fig. 2(a)], $\chi_{\text{nem}}^{[110]}$ is much larger and has a more pronounced temperature dependence as compared with $\chi_{\text{nem}}^{[100]}$. Moreover, as demonstrated previously [15], $\chi_{\text{nem}}^{[110]}$ has a peak at the nematic transition temperature T_{nem} . Above this temperature, the nematic susceptibility can be described by a Curie-Weiss expression

$$\chi_{\text{nem}} = \chi_0 + \frac{C}{T - T_0}. \quad (2)$$

Here, C is a constant, and χ_0 is a temperature-independent term not related to the nematic fluctuations. The Curie-Weiss temperature T_0 represents the “bare” nematic transition temperature without nemo-lattice coupling effects. Such a B_{2g} Ising-nematic order has been observed in many iron-based superconductors [23, 24]. However, in CsFe₂As₂ [Fig. 2(b)], we find that the dominant nematic fluctuations appear in the B_{1g} channel, since $\chi_{\text{nem}}^{[100]}$ displays a considerably larger magnitude and stronger temperature dependence than $\chi_{\text{nem}}^{[110]}$. We also note that the sign of $\chi_{\text{nem}}^{[100]}$ is positive for CsFe₂As₂, in contrast to the negative sign of $\chi_{\text{nem}}^{[110]}$ in BaFe₂As₂. Such a sign reversal has also been reported for the in-plane resistivity anisotropy in Ba_{1-x}K_xFe₂As₂, where the hole doping changes sign of $\rho_b/\rho_a - 1$ from positive to negative [25].

As shown in Fig. 2(c), similar B_{1g} Ising-nematic behavior as in CsFe_2As_2 is also observed in RbFe_2As_2 , suggesting that nematicity along the Fe-As direction, 45° tilted with respect to the Fe-Fe direction, is a generic feature of the $3d^{5.5}$ electronic configuration. Indeed, recent nuclear magnetic resonance and scanning tunneling microscopy studies suggested B_{1g} nematicity in these compounds [26, 27], although the presence of long-range nematic order has not been settled. Here, we note that not only do the $\chi_{\text{nem}}^{[100]}(T)$ curves for both CsFe_2As_2 and RbFe_2As_2 follow Curie-Weiss behavior over a wide temperature range, but also does the nematic susceptibility of RbFe_2As_2 exhibit a distinct peak at $T_{\text{nem}} \sim 38\text{ K}$, indicative of the onset of long-range nematic order in the B_{1g} channel. Recent specific-heat measurements under in-plane field rotation indeed show two-fold oscillations near T_c , supporting the B_{1g} nematic order in RbFe_2As_2 [28]. This is consistent with a positive Curie-Weiss temperature $T_0 \approx 25\text{ K}$ obtained for RbFe_2As_2 by fitting Eq. (2) to $\chi_{\text{nem}}^{[100]}(T)$. In contrast, we have found $T_0 \approx -4\text{ K}$ for CsFe_2As_2 , from which we conclude that CsFe_2As_2 is close to a possible B_{1g} nematic quantum critical point (QCP), which would correspond to $T_0 = 0$. The largely enhanced magnitude of $\chi_{\text{nem}}^{[100]}$ is also consistent with quantum-critical fluctuations of B_{1g} nematicity [24]. We note in passing that, at low temperatures, $\chi_{\text{nem}}^{[100]}$ in CsFe_2As_2 shows a noticeable deviation from the Curie-Weiss behavior. Similar deviations have been seen in several iron-based materials in the vicinity of their putative B_{2g} nematic QCP, when the Curie-Weiss temperature extrapolates to zero [23, 24]. Although disorder effects have been discussed as a possible origin of this behavior, the observation of a similar deviation in the very clean CsFe_2As_2 compound, where sharp quantum oscillations are clearly observed [17], suggests that mechanisms other than disorder may be important for the behavior close to a nematic QCP.

Our elastoresistance measurements thus establish two parent iron-pnictide compounds, the $3d^6$ BaFe_2As_2 and the $3d^{5.5}$ RbFe_2As_2 , that display Ising-nematic orders in two orthogonal channels, namely, B_{2g} (corresponding to $\gamma > 0$ in Eq. (1)) and B_{1g} (corresponding to $\gamma < 0$ in Eq. (1)), respectively. Following the strategy outlined above, we thus search for signatures of XY nematicity in the doped compound $\text{Ba}_{1-x}\text{Rb}_x\text{Fe}_2\text{As}_2$. Note that just because $\text{Ba}_{1-x}\text{Rb}_x\text{Fe}_2\text{As}_2$ interpolates between B_{1g} and B_{2g} nematic orders is not enough to ensure XY nematicity. On the contrary, if these ordered states had completely different origins, one would expect quite generally the B_{1g} fluctuations to be suppressed before B_{2g} fluctuations become sizable (and vice-versa). However, if these two states were manifestations of a common nematic state, differing from each other only in the direction of the nematic director, one would expect XY nematicity to emerge in the regime where the director switches from one direction to the other.

The doping evolution of the elastoresistance is de-

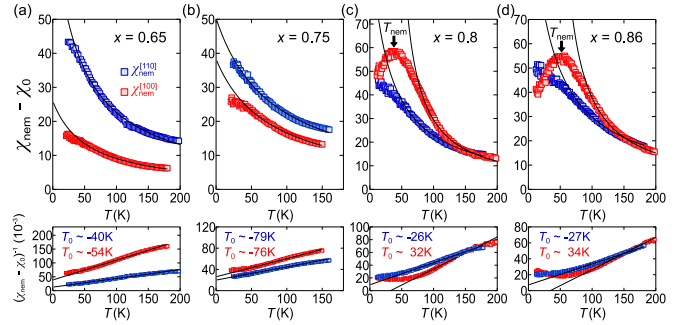


FIG. 3. Nematic susceptibilities in the two symmetry channels $\chi_{\text{nem}}^{[110]}$ (red squares) and $\chi_{\text{nem}}^{[100]}$ (blue squares) for $\text{Ba}_{1-x}\text{Rb}_x\text{Fe}_2\text{As}_2$ single crystals with $x = 0.65$ (a), $x = 0.75$ (b), $x = 0.80$ (c), and $x = 0.86$ (d). To compare the two nematic susceptibilities of each composition, the upper panels show the temperature dependence of $\chi_{\text{nem}} - \chi_0$, with the Curie-Weiss fits (solid lines). The lower panels depict the inverse susceptibilities, from which the Curie-Weiss temperatures are extracted.

picted in Fig. 3(a)-(d). For Rb concentrations up to $x = 0.65$, $\chi_{\text{nem}}^{[110]}$ remains considerably larger than $\chi_{\text{nem}}^{[100]}$. For $x = 0.65$, the temperature dependence of $\chi_{\text{nem}}^{[100]}$ continues to follow a Curie-Weiss behavior with a negative T_0 , indicating the dominance of B_{2g} nematic fluctuations, but there is no evidence for long-range nematic order [Fig. 3(a)]. As the Rb concentration further increases ($x = 0.75, 0.80$, and 0.86), the magnitude of $\chi_{\text{nem}}^{[100]}$ gradually grows at the expense of $\chi_{\text{nem}}^{[110]}$, as shown in Fig. 3(b)-(d), reflecting the development of a B_{1g} nematic instability near $x = 1$. Remarkably, for $x = 0.80$ and 0.86 , the nematic susceptibilities in the two channels have comparable magnitudes and similar temperature dependencies at high temperatures. In this doping range, the system displays long-range B_{1g} nematic order, as signaled by the positive T_0 and, more importantly, by the peak in $\chi_{\text{nem}}^{[100]}(T)$, which defines T_{nem} . Interestingly, despite the onset of long-range order in the B_{1g} channel, $\chi_{\text{nem}}^{[110]}$ continues to increase even below T_{nem} , indicating the importance of both nematic modes for all temperatures. In the x range between B_{1g} and B_{2g} nematic orders, i.e., for $x = 0.75$, the absence of peaks in the nematic susceptibilities indicates the absence of long-range nematic order. In addition, the two nematic susceptibilities show almost identical temperature dependencies, with very similar Curie-Weiss temperatures. The observed comparable Curie-Weiss behavior in these two symmetry-irreducible channels immediately indicates that the nematic fluctuations are isotropic, in contrast to the strongly anisotropic fluctuations found for $x = 0$ and $x = 1$. Note that to establish that the nematic fluctuations are nearly isotropic (i.e. XY-like), it is sufficient to show that the susceptibilities in the two orthogonal channels, B_{1g} and B_{2g} , are very similar. This is because a director pointing along an arbitrary in-plane direction can always be decomposed

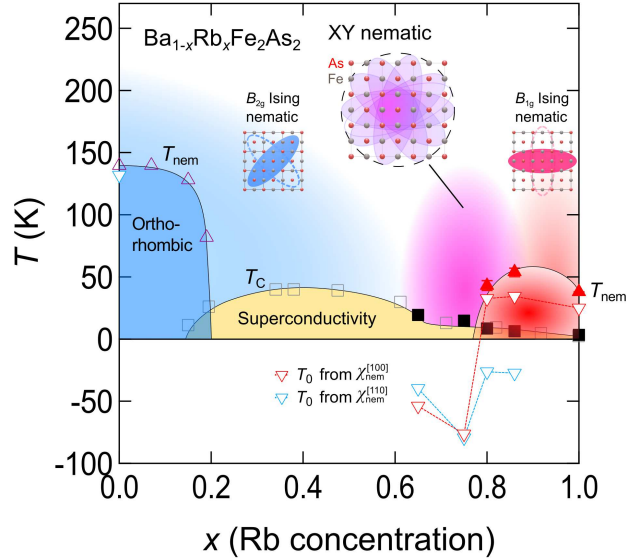


FIG. 4. Temperature (T) versus Rb concentration (x) phase diagram obtained in this study. The structural transition temperature T_{nem} (purple triangles) and the superconducting transition temperature T_c (open squares) refer to previous results on polycrystalline samples [39]. T_c of the single crystals synthesized in this work are denoted by closed squares. The onset temperature T_{nem} (red closed triangles) of the new B_{1g} nematic state is defined by the peak in $\chi_{\text{nem}}^{[100]}$. The Curie-Weiss temperatures T_0 are extracted from the Curie-Weiss fittings of $\chi_{\text{nem}}^{[100]}$ (red inverted triangles) and $\chi_{\text{nem}}^{[110]}$ (blue inverted triangles). The lines are guides to the eyes. The blue, red, and purple shaded regions highlight the three different types of nematic fluctuations observed above the ordering temperatures.

as a linear combination of the B_{1g} director and the B_{2g} director. The situations is analogous to the case of a nearly-XY ferromagnet, which displays comparable susceptibilities χ_{FM}^{xx} and χ_{FM}^{yy} . Thus, our results provide direct evidence that the $x = 0.75$ concentration is very close to an XY-nematic state.

Our main findings are summarized in the $\text{Ba}_{1-x}\text{Rb}_x\text{Fe}_2\text{As}_2$ phase diagram shown in Fig. 4. The electronic nematic director rotates by 45° with increasing Rb doping, changing from B_{2g} Ising-nematic order near $x = 0$ (blue region) to B_{1g} Ising-nematic order at $x = 1$ (red region). In an intermediate doping range, the nematic susceptibilities in the two channels become very similar, thus revealing an emergent nearly-XY nematic fluctuating regime (purple region). The Curie-Weiss temperature extracted from the B_{1g} nematic susceptibility shows an abrupt change near the $x = 0.80$ composition, below which long-range B_{1g} nematic order is no longer detected. It is noteworthy that in the related compound $\text{Ba}_{1-x}\text{K}_x\text{Fe}_2\text{As}_2$, the Fermi pockets near the Brillouin zone corner change from electron-like to hole-like near a similar doping composition [29].

Our results offer important new insights about the mi-

croscopic mechanism of nematicity in iron-based superconductors. More specifically, one can envision two possible general theoretical scenarios to explain our results. In the first scenario, both the B_{2g} and B_{1g} nematic states have the same origin. Given the evidence in favor of a magnetically-driven B_{2g} nematic state for the $x = 0$ compound [30], the question is whether magnetic fluctuations can also promote B_{1g} nematicity. In this regard, recent works have proposed that the wave-vector \mathbf{Q} of the dominant magnetic fluctuations change from being parallel to the Fe-Fe direction for $x = 0$ to being parallel to the Fe-As direction for $x = 1$ [31, 32]. This would naturally lead to a change in the vestigial nematic order from B_{2g} to B_{1g} [33, 34]. Indeed, first-principle calculations [31] predict that the magnetic ground state changes from single-stripe, $\mathbf{Q} = (\pi, \pi)$, for $x = 0$, to double-stripe, $\mathbf{Q} = (\pi, 0)$, for $x = 1$ (recall that we are referring to the crystallographic 2-Fe unit cell). A related theoretical proposal also attributes the change in nematicity to a change in the magnetic spectrum, which would become incommensurate due to the occurrence of a Lifshitz transition as $x = 1$ is approached [35]. While long-range magnetic order has not been observed in RbFe_2As_2 , inelastic neutron scattering measurements, which probe directly the magnetic fluctuation spectrum, could be used to verify the applicability of this type of scenarios.

An alternative scenario is that the two nematic states have different origins. In this context, recent studies of possible charge order in RbFe_2As_2 [36] and in KFe_2As_2 under high pressure [37] suggest that charge degrees of freedom could be important. Moreover, a distinguishing feature of the $x = 1$ compound, and of all $3d^{5.5}$ stoichiometric compounds, is the proposed enhanced strength of electronic correlations [16–21]. One interesting possibility then is that the B_{1g} nematic state in RbFe_2As_2 could be the result of a symmetry-breaking Kondo-like hybridization gap between the more localized d_{xy} orbital and the more itinerant d_{xz} , d_{yz} orbitals [38]. Another possibility would be ferro-orbital order involving the d_{xz} , d_{yz} orbitals only, although a microscopic mechanism that does not involve magnetic fluctuations has yet to be proposed.

IV. CONCLUSIONS

From the elastoresistance measurements in $\text{Ba}_{1-x}\text{Rb}_x\text{Fe}_2\text{As}_2$, it is found that the nematic director rotates from Fe-Fe to Fe-As directions with hole doping. In the intermediate doping regimes, the nematic susceptibilities in the two symmetry-irreducible (B_{1g} and B_{2g}) channels show very similar Curie-Weiss behavior, indicating nearly isotropic nematic fluctuations that are different from the Ising nematicity found in other iron-based superconductors.

The present observation of electronic XY-nematic fluctuations in overdoped $\text{Ba}_{1-x}\text{Rb}_x\text{Fe}_2\text{As}_2$ offers a new route to realizing this novel quantum liquid-crystalline

state in iron-based superconductors. A promising direction is attempting to stabilize long-range XY-nematic order, for instance by combining chemical substitution and application of pressure [31]. One of the unique properties of such an XY-nematic state is that its Goldstone mode couples directly to the electronic density, as discussed above. Of course, the system will inevitably have a small anisotropy favoring one of the two nematic components, which will gap the Goldstone mode. Yet, for a small anisotropy, as implied by our elastoresistance data for the $x = 0.75$ composition, much of the system's behavior (except at very low energies) is similar to that of a true XY-nematic state.

ACKNOWLEDGEMENTS

We thank fruitful discussion with A. E. Böhmer, V. Borisov, A. Chubukov, A. Fujimori, Y. Gallais, H. Kontani, C. Meingast, S. Onari, J. C. Palmstrom, I. Paul, J. Schmalian, Q. Si, and R. Valenti. This work was supported by “Kakehashi” collaborative research program of Tsukuba Innovation Arena and by Grants-in-Aid for Scientific Research (Nos. 15H02106, 18H05227, 18K13492) from Japan Society for the Promotion of Science. X-ray diffraction measurements were partly supported by the joint research in the Institute for Solid State Physics, the University of Tokyo. Theory work (R.M.F.) was supported by the U.S. Department of Energy, Office of Science, Basic Energy Sciences, under Award No. DE-SC0012336.

APPENDIX A: SINGLE CRYSTALS

Single crystals of RbFe_2As_2 and CsFe_2As_2 were grown from arsenic-rich flux as described in Ref. 17. The crystals grown by this method have been characterized by several measurements including X-ray, thermal expansion, ac susceptibility, and specific heat [17–19], and quantum oscillations have been observed in the magnetostriction [17] indicating the cleanliness of these samples. Single crystals of $\text{Ba}_{1-x}\text{Rb}_x\text{Fe}_2\text{As}_2$ with various Rb concentrations x were grown by the FeAs self-flux method [40]. x was determined by energy dispersive X-ray spectrometry and also checked from the c -axis lattice constant measured by X-ray diffraction. The temperature dependence of the in-plane resistivity is measured by the standard four-probe method, and the results of $\text{Ba}_{1-x}\text{Rb}_x\text{Fe}_2\text{As}_2$ single crystals are shown in Fig. 5. The superconducting transition temperature T_c of the crystals was determined by the onset of superconducting transition (black arrows). The characteristic S-shaped temperature dependence as well as overall doping dependence of T_c are similar to that reported in $\text{Ba}_{1-x}\text{K}_x\text{Fe}_2\text{As}_2$ single crystals [41].

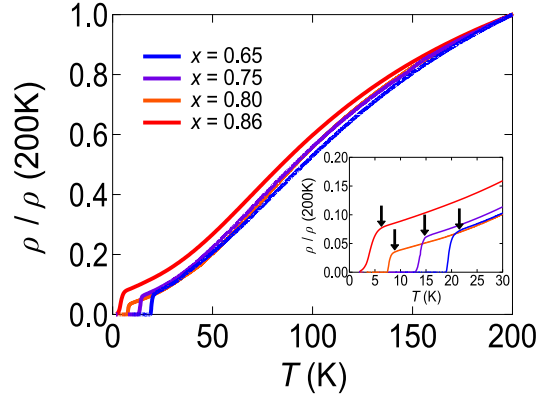


FIG. 5. Temperature dependence of the resistivity for the $\text{Ba}_{1-x}\text{Rb}_x\text{Fe}_2\text{As}_2$ single crystals. The vertical axis is normalized by the resistivity value at 200 K. The inset shows an expanded view below 30 K. The arrows indicate the onset of superconducting transition.

APPENDIX B: NEMATIC SUSCEPTIBILITY MEASUREMENTS

We have systematically evaluated the B_{1g} and B_{2g} nematic susceptibility in $A\text{Fe}_2\text{As}_2$ ($A = \text{Ba}, \text{Cs}$ and Rb) and $\text{Ba}_{1-x}\text{Rb}_x\text{Fe}_2\text{As}_2$ (Figs. 2 and 3) from longitudinal elastoresistance measurements, where the current direction is parallel to the applied strain ϵ_{xx} . At present, we have not obtained reliable data for KFe_2As_2 , whose crystals are more sensitive to air.

For the longitudinal measurements we use rectangular crystals with typical dimensions of $\sim 1.0 \times 0.4 \times 0.02 \text{ mm}^3$. The resistance of the sample (R_{xx}) was measured by the conventional four-probe method [Fig. 6(a)]. For the B_{1g} and B_{2g} nematic susceptibility measurements, the edges of the samples are aligned along the tetragonal [100] and [110] directions, respectively.

It should be noted that, strictly speaking, the strain

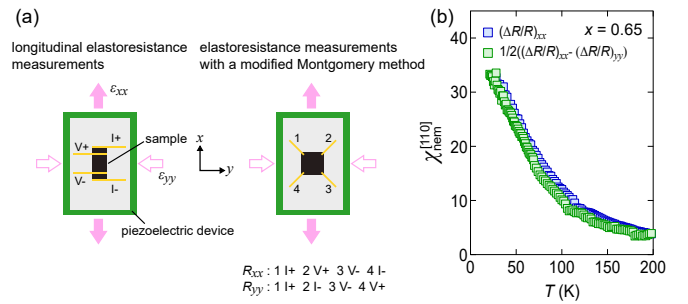


FIG. 6. Biaxial strain effect to the nematic susceptibility. (a) Schematic illustration of the two elastoresistance measurements. (b), The temperature dependence of $\chi_{\text{nem}}^{[110]}$ for $\text{Ba}_{1-x}\text{Rb}_x\text{Fe}_2\text{As}_2$ with $x = 0.65$ obtained by longitudinal elastoresistance measurements (blue square), which is the same data as in Fig. 3(a), and by a modified Montgomery method (green square).

transmitted to the sample via the orthorhombic deformation of the piezoelectric stack has not uniaxial but highly anisotropic biaxial character, which can be decomposed into in-plane A_{1g} -symmetry strain ($\frac{1}{2}(\epsilon_{xx} + \epsilon_{yy})$) and $B_{1g/2g}$ -symmetry strain ($\frac{1}{2}(\epsilon_{xx} - \epsilon_{yy})$). However, since ϵ_{xx} and ϵ_{yy} have opposite signs, and their ratio is characterized by the in-plane Poisson's ratio ν_p of the piezoelectric device ($\epsilon_{yy} = -\nu_p \epsilon_{xx}$), the A_{1g} -symmetry strain is small compared to the $B_{1g/2g}$ -symmetry strain [42]. To see the effect of A_{1g} -symmetry strain on the elastoresistance, we also conducted additional elastoresistance measurements using a modified Montgomery method [23]. For this type of measurement, samples with

square shape were used ($\sim 0.6 \times 0.6 \times 0.03 \text{ mm}^3$), and the resistances along both x and y directions (R_{xx} and R_{yy}) are measured by switching the current and voltage configurations [Fig. 6(a)]. In this method, the nematic susceptibility χ_{nem} is given by $\chi_{\text{nem}} \sim (1/2((\Delta R/R)_{xx} - (\Delta R/R)_{yy}))/\epsilon_{xx}$, in which A_{1g} -symmetry strain effect can be removed.

As shown in Fig. 6(b), the data of $\chi_{\text{nem}}^{[110]}(T)$ in $\text{Ba}_{1-x}\text{Rb}_x\text{Fe}_2\text{As}_2$ with $x = 0.65$ determined by two methods are almost identical, revealing that the A_{1g} -symmetry strain effect is negligibly small in the present measurements, and the longitudinal elastoresistance measurements can be used to extract nematic susceptibility in our study.

-
- [1] E. Fradkin, S. A. Kivelson, M. J. Lawler, J. P. Eisenstein, and A. P. Mackenzie, *Nematic Fermi fluids in condensed matter physics*, Annu. Rev. Condens. Matter Phys. **1**, 153-178 (2010).
- [2] R. M. Fernandes, A. V. Chubukov, and J. Schmalian, *What drives nematic order in iron-based superconductors?*, Nat. Phys. **10**, 97-104 (2014).
- [3] M. P. Lilly, K. B. Cooper, J. P. Eisenstein, L. N. Pfeiffer, and K. W. West, *Evidence for an anisotropic state of two-dimensional electrons in high Landau levels*, Phys. Rev. Lett. **82**, 394-397 (1999).
- [4] J.-H. Chu *et al.*, *In-plane resistivity anisotropy in an underdoped iron arsenide superconductor*, Science **329**, 824-826 (2010).
- [5] S. Kasahara. *et al.*, *Electronic nematicity above the structural and superconducting transition in $\text{BaFe}_2(\text{As}_{1-x}\text{P}_x)_2$* , Nature **486**, 382-385 (2012).
- [6] S. Lederer, Y. Schattner, E. Berg, and S. A. Kivelson, *Superconductivity and non-Fermi liquid behavior near a nematic quantum critical point*, Proc. Natl. Acad. Sci. USA **114**, 4905-4910 (2016).
- [7] V. Hinkov *et al.*, *Electronic liquid crystal state in the high-temperature superconductor $\text{YBa}_2\text{Cu}_3\text{O}_{6.45}$* , Science **319**, 597-600 (2008).
- [8] R. Daou *et al.*, *Broken rotational symmetry in the pseudogap phase of a high- T_c superconductor*, Nature **463**, 519-522 (2010).
- [9] Y. Sato *et al.*, *Thermodynamic evidence for a nematic phase transition at the onset of the pseudogap in $\text{YBa}_2\text{Cu}_3\text{O}_y$* , Nat. Phys. **13**, 1074-1078 (2017).
- [10] R. Okazaki *et al.*, *Rotational symmetry breaking in the hidden-order phase of URu_2Si_2* , Science **331**, 439-442 (2011).
- [11] V. Oganesyan, S. A. Kivelson, and E. Fradkin, *Quantum theory of a nematic Fermi fluid*, Phys. Rev. B **64**, 195109 (2001).
- [12] M. Zacharias, P. Wölfle, and M. Garst, *Multiscale quantum criticality: Pomeranchuk instability in isotropic metals*, Phys. Rev. B **80**, 165116 (2009).
- [13] H. Watanabe and A. Vishwanath, *A. Criterion for stability of Goldstone modes and Fermi liquid behavior in a metal with broken symmetry*, Proc. Natl. Acad. Sci. USA **111**, 16314-16318 (2014).
- [14] Y. B. Kim and H.-Y. Kee, *Pairing instability in a nematic Fermi liquid*, J. Phys.: Condens. Matt. **16**, 3139-3145 (2004).
- [15] J. -H. Chu, H.-H. Kuo, J. G. Analytis, and I. R. Fisher, *Divergent nematic susceptibility in an iron arsenide superconductor*, Science **337**, 710-712 (2012).
- [16] F. Hardy *et al.*, *Evidence of strong correlations and coherence-incoherence crossover in the iron pnictide superconductor $K\text{Fe}_2\text{As}_2$* , Phys. Rev. Lett. **111**, 027002 (2013).
- [17] F. Eilers *et al.*, *Strain-driven approach to quantum criticality in $A\text{Fe}_2\text{As}_2$ with $A = K, \text{Rb}$, and Cs* , Phys. Rev. Lett. **116**, 237003 (2016).
- [18] F. Hardy *et al.*, *Strong correlations, strong coupling, and s-wave superconductivity in hole-doped BaFe_2As_2 single crystals*, Phys. Rev. B **94**, 205113 (2016).
- [19] Y. Mizukami *et al.*, *Evolution of quasiparticle excitations with enhanced electron correlations in superconducting $A\text{Fe}_2\text{As}_2$ ($A = K, \text{Rb}, \text{Cs}$)*, Phys. Rev. B **94**, 024508 (2016).
- [20] L. de' Medici, G. Giovannetti, and M. Capone, *Selective Mott physics as a key to iron superconductors*, Phys. Rev. Lett. **112**, 177001 (2014).
- [21] S. Backes, H. O. Jeschke, and R. Valenti, *Microscopic nature of correlations in multiorbital $A\text{Fe}_2\text{As}_2$ ($A=K, \text{Rb}, \text{Cs}$): Hund's coupling versus Coulomb repulsion*, Phys. Rev. B **92**, 195128 (2015).
- [22] S. A. Kivelson, E. Fradkin, and V. J. Emery, *Electronic liquid-crystal phases of a doped Mott insulator*, Nature **393**, 550-553 (1998).
- [23] H. -H. Kuo, J.-H. Chu, S. A. Kivelson, and I. R. Fisher, *Ubiquitous signatures of nematic quantum criticality in optimally doped Fe-based superconductors*, Science **352**, 958-962 (2016).
- [24] S. Hosoi *et al.*, *Nematic quantum critical point without magnetism in $\text{FeSe}_{1-x}\text{S}_x$ superconductors*, Proc. Natl. Acad. Sci. USA **113**, 8139-8143 (2016).
- [25] E. C. Blomberg *et al.*, *Sign-reversal of the in-plane resistivity anisotropy in hole-doped iron pnictides*, Nat. Commun. **4**, 1914 (2013).
- [26] J. Li *et al.*, *Reemerging electronic nematicity in heavily hole-doped Fe-based superconductors*, arXiv:1611.04694.
- [27] X. Liu *et al.*, *Evidence of nematic order and nodal superconducting gap along [110] direction in RbFe_2As_2* , arXiv:1803.07304.

- [28] O. Tanaka *et al.*, (unpublished); *Specific heat evidence for rotational symmetry breaking in RbFe₂As₂*, Presented at APS March Meeting (2019).
- [29] N. Xu *et al.*, *Possible nodal superconducting gap and Lifshitz transition in heavily hole-doped Ba_{0.1}K_{0.9}Fe₂As₂*, Phys. Rev. B **88**, 220508(R) (2013).
- [30] R. M. Fernandes, A. E. Böhmer, C. Meingast, and J. Schmalian, *Scaling between magnetic and lattice fluctuations in iron pnictide superconductors*, Phys. Rev. Lett. **111**, 137001 (2013).
- [31] V. Borisov, R. M. Fernandes, and R. Valenti, *Evolution from B_{2g} nematics to B_{1g} nematics in heavily hole-doped iron-based superconductors*, arXiv:1902.10729.
- [32] Y. Wang, W. Hu, R. Yu, and Q. Si, *Broken mirror symmetry, incommensurate spin correlations, and B_{2g} nematic order in iron pnictides*, arXiv:1903.00375.
- [33] G. Zhang, J. K. Glasbrenner, R. Flint, I. I. Mazin, and R. M. Fernandes, *Double-stage nematic bond ordering above double stripe magnetism: Application to BaTi₂Sb₂O*, Phys. Rev. B **95**, 174402 (2017).
- [34] C. B. Bishop, J. Herbrych, E. Dagotto, and A. Moreo, *Possible bicolinear nematic state with monoclinic lattice distortions in iron telluride compounds*, Phys. Rev. B **96**, 035144 (2017).
- [35] S. Onari and H. Kontani, *Origin of diverse nematic orders in Fe-based superconductors: 45° rotated nematicity in AFe₂As₂ (A = Cs, Rb)*, arXiv:1809.08017.
- [36] E. Civardi, M. Moroni, M. Babij, Z. Bukowski, and P. Carretta, *Superconductivity emerging from an electronic phase separation in the charge ordered phase of RbFe₂As₂*, Phys. Rev. Lett. **117**, 217001 (2016).
- [37] P. S. Wang *et al.*, *Nearly critical spin and charge fluctuations in KFe₂As₂ observed by high-pressure NMR*, Phys. Rev. B **93**, 085129 (2016).
- [38] J. Schmalian, *private communication*.
- [39] S. Peschke, T. Stürzer, and D. Johrendt, *Ba_{1-x}Rb_xFe₂As₂ and generic phase behavior of hole-doped 122-type superconductors*, J. Inorg. Gen. Chem. **640**, 830 (2014).
- [40] M. Tsujii *et al.*, (unpublished).
- [41] Y. Liu *et al.*, *Comprehensive scenario for single-crystal growth and doping dependence of resistivity and anisotropic upper critical fields in (Ba_{1-x}K_x)Fe₂As₂ (0.22 ≤ x ≤ 1)*, Phys. Rev. B **89**, 134504 (2014).
- [42] H.-H. Kuo, M. C. Shapiro, S. C. Riggs, and I. R. Fisher, *Measurement of the elastoresistivity coefficients of the underdoped iron arsenide Ba(Fe_{0.975}Co_{0.025})₂As₂*, Phys. Rev. B **88**, 085113 (2013).